Binary crystals in two-dimensional two-component Yukawa mixtures

Lahcen Assoud, René Messina, Hartmut Löwen

Institut für Theoretische Physik II: Weiche Materie,

Heinrich-Heine-Universität Düsseldorf,

Universitätsstrasse 1, D-40225 Düsseldorf, Germany

(Dated: February 2, 2008)

Abstract

The zero-temperature phase diagram of binary mixtures of particles interacting via a screened Coulomb pair potential is calculated as a function of composition and charge ratio. The potential energy obtained by a Lekner summation is minimized among a variety of candidate two-dimensional crystals. A wealth of different stable crystal structures is identified including A, B, AB_2, A_2B, AB_4 structures [A (B) particles correspond to large (small) charge.] Their elementary cells consist of triangular, square or rhombic lattices of the A particles with a basis comprising various structures of A and B particles. For small charge asymmetry there are no intermediate crystals besides the pure A and B triangular crystals. The predicted structures are detectable in experiments on confined mixtures of charged colloids or dusty plasma sheets.

PACS numbers: 82.70.Dd, 61.50.Ah, 61.66.Dk

I. INTRODUCTION

Two-component mixtures in general exhibit much richer crystallization phenomena and polymorphism than their one-component counterparts [1] as witnessed by a huge variety of possible stable binary crystals, e.g. for binary hard sphere systems [2, 3, 4, 5]. How the whole crystal phase behavior in mixtures depends on the interparticle interactions is far from being understood even in equilibrium [6, 7]. This is true also in two spatial dimensions where the number of Bravais lattices is smaller than in three dimensions. Binary mixtures in two dimensions have been studied for hard disks [8] and a complex diagram of close packing was obtained as a function of their diameter ratio. More recently, a two-dimensional binary mixture with soft interactions was considered [9], namely that for parallel dipoles where the pair potential scales with the inverse cube of the interparticle separation. A variant of this model has been considered in Ref. [10]. Such systems can be realized in granular matter [11] and in magnetic colloidal suspensions confined to a air-water interface [12]. Again, as a function of the ratio of dipole moments of the two species, a complex stability phase diagram of stable binary crystals was obtained that qualitatively differs from the hard disk case [8]. In particular for low asymmetries, the hard disk system shows a complete separation into pure A and B triangular crystals [8] while the soft dipolar systems possesses two stable mixed crystals as well with stoechiometric ratio A_2B and AB_2 [9]. These differences show that the topology of the phase diagrams depend on details of the interactions and there is certainly a need to understand this dependence in more detail.

In this paper, we consider a two-dimensional binary system of Yukawa particles, i.e. the pair interaction potential $V(r)$ between the particles is a screened Coulomb interaction $\propto \exp(\kappa r)/r$ where κ is the screening constant (or the inverse screening length). This potential interpolates between the case of hard disks (as obtained in the limit of high κ) and the unscreened Coulomb case (as obtained for $\kappa = 0$). The latter limit, $V(r) \propto 1/r$ is even softer than the dipolar case where $V(r) \propto 1/r^3$. The two components are defined by two different charges, i.e. different prefactors in front of the Yukawa interaction. In previous works, such a classical binary mixture with Yukawa interactions in three-dimensions has been used as a model to study mixing rules [13], effective forces [14], fluid-fluid phase separation [15, 16, 17], dynamical correlations [18, 19] and transport properties [20]. Likewise the pure (one-component) Yukawa system was also studied in two-spatial dimensions for fluid

structure [21, 22, 23, 24], dynamics [25, 26, 27, 28] and transport properties [29]. Binary mixtures of Yukawa particles in two dimensions have also been studied for fluid structure [30], adsorption [31], interfaces [32] and transport [33]. However, the crystallization issue was only addressed in one-component Yukawa systems (for a recent work, see e.g. [34]) but never in binary mixtures.

The Yukawa potential is realized in *charged colloidal suspensions* [35] as well as in *dusty plasmas* [36], both for one component systems and mixtures. In fact, highly charged colloidal suspensions can be confined between highly charged parallel glass plates [37, 38, 39] which restricts their motion practically to two dimensions. The interactions between these macroions are screened due to the presence of the microscopic microions and additional salt ions. As in three dimensions, the Debye-Hückel screened Coulomb interaction is a reasonable model for confined charged colloids [40, 41]. Crystallization of binary charged colloids has been studied experimentally in the bulk. However, a monolayer of a confined binary mixture of charged colloids has not yet been realized although this is in principle possible as has been shown for sterically-stabilized [42] and magnetic colloids [43]. On the other hand, sheets of highly charged dust particles in plasmas (so-called complex plasmas) can also be confined to two dimensions, e.g. by levitating electric fields. The interaction between the dust particles is again screened such that a Yukawa model is appropriate [36, 44, 45]. Highly charged microspheres suspended in a plasma settled in a horizontal monolayer were studied experimentally and compared to a two-dimensional Yukawa model [46, 47, 48]. There is no principle problem in studying binary mixtures of dust particles but a concrete realization in an experiments still has to be performed as well.

Apart from its important realizations, our major motivation for our studies is to understand the interplay between the interparticle interaction and the stability of different two-dimensional crystal lattices. A control of colloidal composite lattices may lead to new photonic crystals [49] to molecular-sieves [50] and to micro- and nano-filters with desired porosity [51]. The electric properties of a nanocrystal depend on its superlattice structure [52]. For these type of applications, it is crucial to understand the various stable lattice types in binary mixtures.

For the two-component two-dimensional Yukawa mixture, we obtain the full phase diagram at zero-temperature as a function of the charge asymmetry using lattice sums. As a result, we find a variety of different stable composite lattices. They include

A, B, AB_2, A_2B, AB_4 structures. Their elementary cells consist of (equilateral) triangular, square and rhombic lattices of the big particles. These are highly decorated by a basis involving either A particles alone or both B and A particles. The topology of the resulting phase diagram differs qualitatively from that of hard disk mixtures [8] and dipoles [9].

The paper is organized as follows: In Sec. II the model is described and possible candidate structures for crystal lattices in two dimensions are proposed. Results for the phase diagrams are presented in Sec. III. We conclude finally in Sec. IV.

II. MODEL

The model systems used in our study are binary mixtures of (repulsive) charged particles made up of two species denoted as A and B. Each component A and B is characterized by its charge valency Z_A and Z_B, respectively. These constitutive particles are confined to a two-dimensional plane, and interact via the Yukawa pair potential. Introducing the ratio $Z = Z_B/Z_A$ the pair interaction potentials between two A particles, a A- and B-particles, and two B-particle at distance r are

$$\begin{aligned} V_{AA}(r) &= \kappa V_0 \varphi(r), \quad V_{AB}(r) = \kappa V_0 Z \varphi(r), \\ V_{BB}(r) &= \kappa V_0 Z^2 \varphi(r), \end{aligned} \tag{1}$$

respectively. The dimensionless function $\varphi(r)$ is given by

$$\varphi(r) = \frac{\exp(-\kappa r)}{\kappa r}, \tag{2}$$

where the energy amplitude $V_0\kappa$ sets the energy scale.

Our goal is to determine the stable crystalline structures adopted by the system at zero temperature. We consider a parallelogram as a primitive cell which contains n_A A-particles and n_B B-particles. This cell can be described geometrically by the two lattice vectors $\mathbf{a} = a(1, 0)$ and $\mathbf{b} = a\gamma(\cos\theta, \sin\theta)$, where θ is the angle between $\mathbf{a}$ and $\mathbf{b}$ and γ is the aspect ratio ($\gamma = |\mathbf{b}|/|\mathbf{a}|$). The position of a particle i (of species A) and that of a particle j (of species B) in the parallelogram is specified by the vectors $\mathbf{r}_{\mathrm{i}}^A = (x_i^A, y_i^A)$ and $\mathbf{r}_{\mathrm{j}}^B = (x_j^B, y_j^B)$, respectively. The total internal energy (per primitive cell) U has the form

$$U = \frac{1}{2} \sum_{J=A,B} \sum_{i,j=1}^{n_J} {\sum_{\mathbf{R}}}' V_{JJ} \left(\left| \mathbf{r}_i^J - \mathbf{r}_j^J + \mathbf{R} \right| \right) + \sum_{i=1}^{n_A} \sum_{j=1}^{n_B} \sum_{\mathbf{R}} V_{AB}(\left| \mathbf{r}_i^A - \mathbf{r}_j^B + \mathbf{R} \right|), \tag{3}$$

where $\mathbf{R} = k\mathbf{a} + l\mathbf{b}$ with k and l being integers. The sums over $\mathbf{R}$ in Eq. 3 run over all lattice cells where the prime indicates that for $\mathbf{R} = 0$ the terms with $i = j$ are to be omitted. In order to handle efficiently the long-range nature of the Yukawa interaction at moderate screening strength, we employed a Lekner-summation (see Appendix A).

We choose to work at prescribed pressure p and zero temperature ($T = 0$). Hence, the corresponding thermodynamic potential is the Gibbs free energy G. Additionally, we consider interacting particles at composition $X := n_B/(n_A + n_B)$, so that the (intensive) Gibbs free energy g per particle reads: $g = g(p, Z, X) = G/(n_A + n_B)$. At vanishing temperature, g is related to the internal energy per particle $u = U/(n_A + n_B)$ through $g = u + p/\rho$, where the pressure p is given by $p = \rho^2(\partial u/\partial\rho)$, and $\rho = (n_A + n_B)/|\mathbf{a} \times \mathbf{b}|$ is the total particle density. The Gibbs free energy per particle g has been minimized with respect to γ, θ and the position of particles of species A and B within the primitive cell. In order to decrease the complexity of the energy landscape, we have limited the number of variables and considered the following candidates for our binary mixtures: A_4B, A_3B, A_2B, A_4B_2, A_3B_2, AB, A_2B_2, A_3B_3, A_2B_3, AB_2, A_2B_4, AB_3, AB_4 and AB_6. For the AB_6 and A_3B_3 case we have only considered a triangular lattice formed by the A particles.

III. RESULTS

A. Phase diagram

The ultimate phase diagrams in the (Z, X) plane has been obtained by employing the Maxwell construction. We recall here that the both dimensionless quantities, namely the charge ratio Z as well as the composition X, can vary between zero and unity. A low charge ratio (i.e., Z is close to zero) indicates a strong charge asymmetry, whereas a high charge ration (i.e., Z is close to unity) represents a large charge symmetry or equivalently a weak charge asymmetry. Given the fact that the phase behavior is getting increasingly

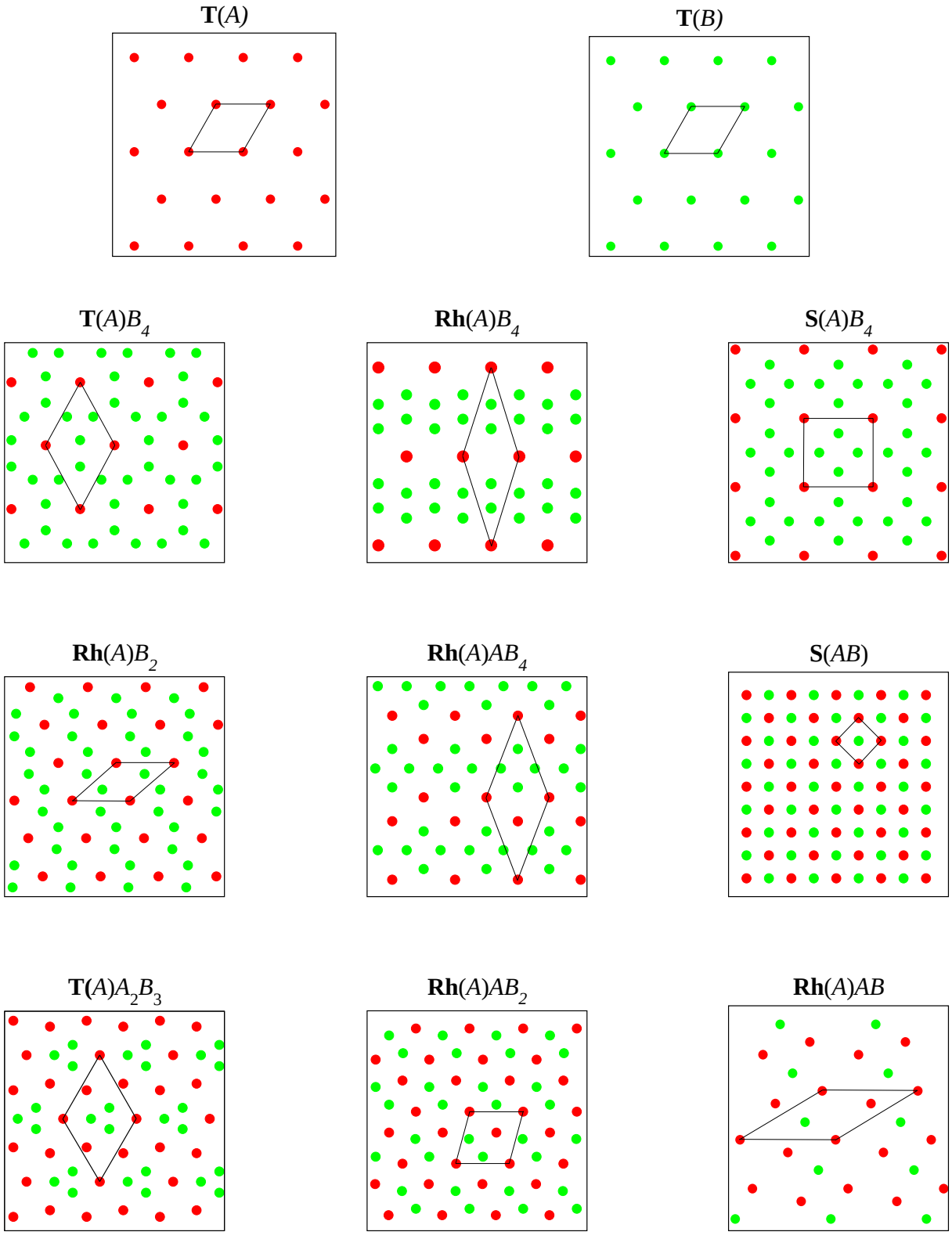

FIG. 1: The stable binary crystal structures and their primitive cells. The red (green) discs correspond to A (B) particles.

TABLE I: The stable phases with their Bravais lattice and their basis.

Phase	Bravais lattice [basis]
$\mathbf{T}(A)$	Triangular for A [one A particle]
$\mathbf{T}(B)$	Triangular for B [one B particle]
$\mathbf{S}(AB)$	Square for A and B together [one A and one B particles]
$\mathbf{S}(A)B_n$	Square for A [one A and n B particles]
$\mathbf{Rh}(A)A_mB_n$	Rhombic for A [$(m+1)$ A and n B particles]
$\mathbf{T}(A)A_mB_n$	Triangular for A [$(m+1)$ A and n B particles]

complicated upon lowering Z, involving a huge basket of candidates, we only present results starting from $Z = 0.2$. Furthermore, in contrast to situations where the pair potential can be described as a power low of the separation distance (as it was the case in our previous work on dipolar mixtures [9]), the phase diagram becomes pressure dependent for Yukawa systems. To capture this feature, we present results at three well distinct pressures, namely $p^* \equiv p/(V_0\kappa^3) = 0.01, 1$ and 100. An overview of the resulting stable crystalline phases can be found in Fig. 1. The corresponding nomenclature of the phase labeling is explained in Table I. The phase diagrams in the (Z, X) plane for the three reduced pressures $p^* = 0.01, 1$ and 100 are depicted in Fig. 2(a), Fig. 2(b), and Fig. 2(c), respectively. Note that upon increasing p^* at prescribed Z and X one decreases the density.

Let us first focus our discussion on the apparently simple phase behavior reported at weak charge asymmetry (here roughly $Z \gtrsim 0.5$, see Fig. 2). Thereby, the system phase separates into a pure A-triangular crystalline phase and a B-one (see also Fig. 1). This triangular structure obviously corresponds to the single-component ground-state. Having in mind that the same phase behavior is reported for hard disks binary mixtures at small size asymmetry [8], it is meaningful to equally expect a phase separation for moderate or sufficiently large reduced screening strength $\kappa^* \equiv \kappa/\sqrt{\rho}$. For $Z = 1$, we have $\kappa^* \approx 3.0, 1.2, 0.4$ for $p^* = 0.01, 1, 100$, respectively, so that the phase separation is certainly to be expected for moderate pressures (here $p^* = 0.01$ and possibly $p^* = 1$) when referring to the hard disk limit [8].

What is now less obvious, still in the regime of weak charge asymmetry, is the phase

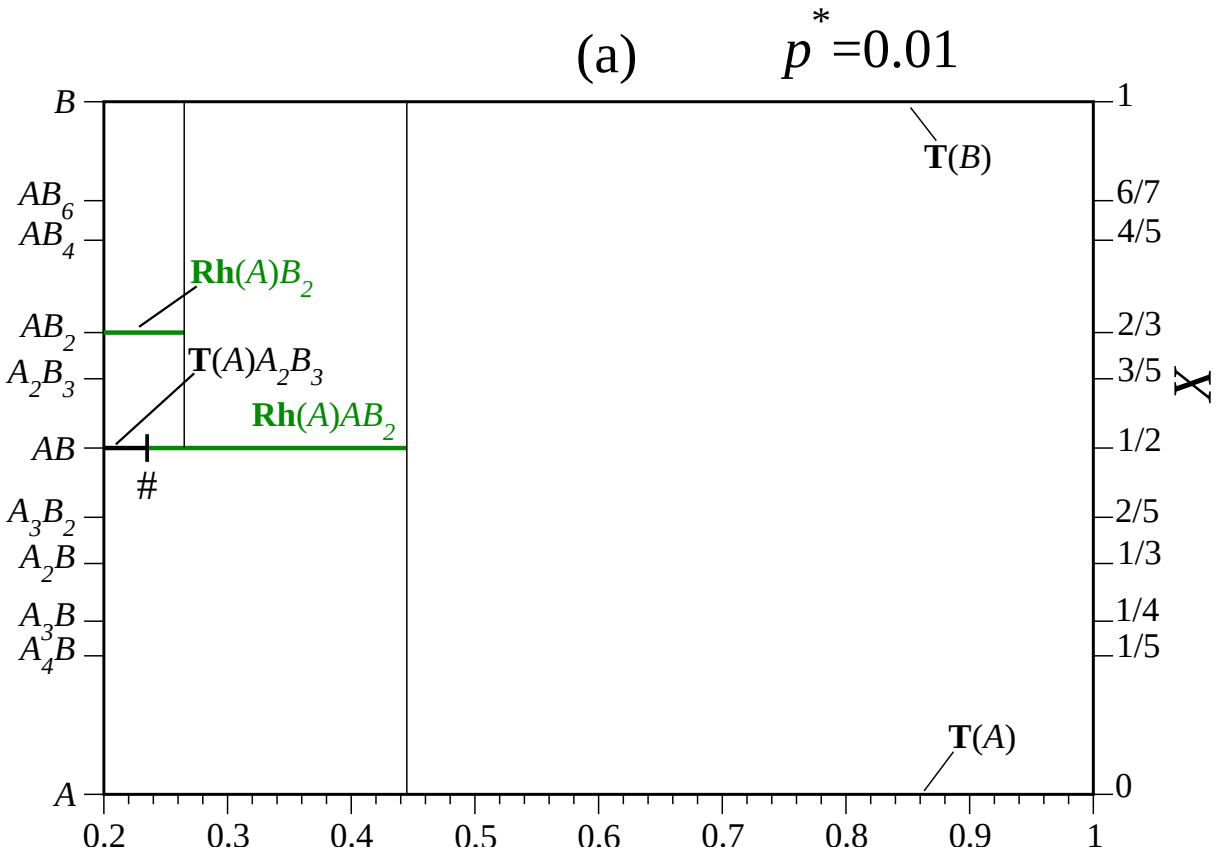
(a)
p^*=0.01
B
AB6
AB4
AB2
A2B3
AB
A3B2
A2B
A3B
A4B
A
1
6/7
4/5
2/3
3/5
1/2
2/5
1/3
1/4
1/5
0
T(B)
T(A)
Rh(A)B2
T(A)A2B3
Rh(A)AB2
#
0.2
0.3
0.4
0.5
0.6
0.7
0.8
0.9
1
X

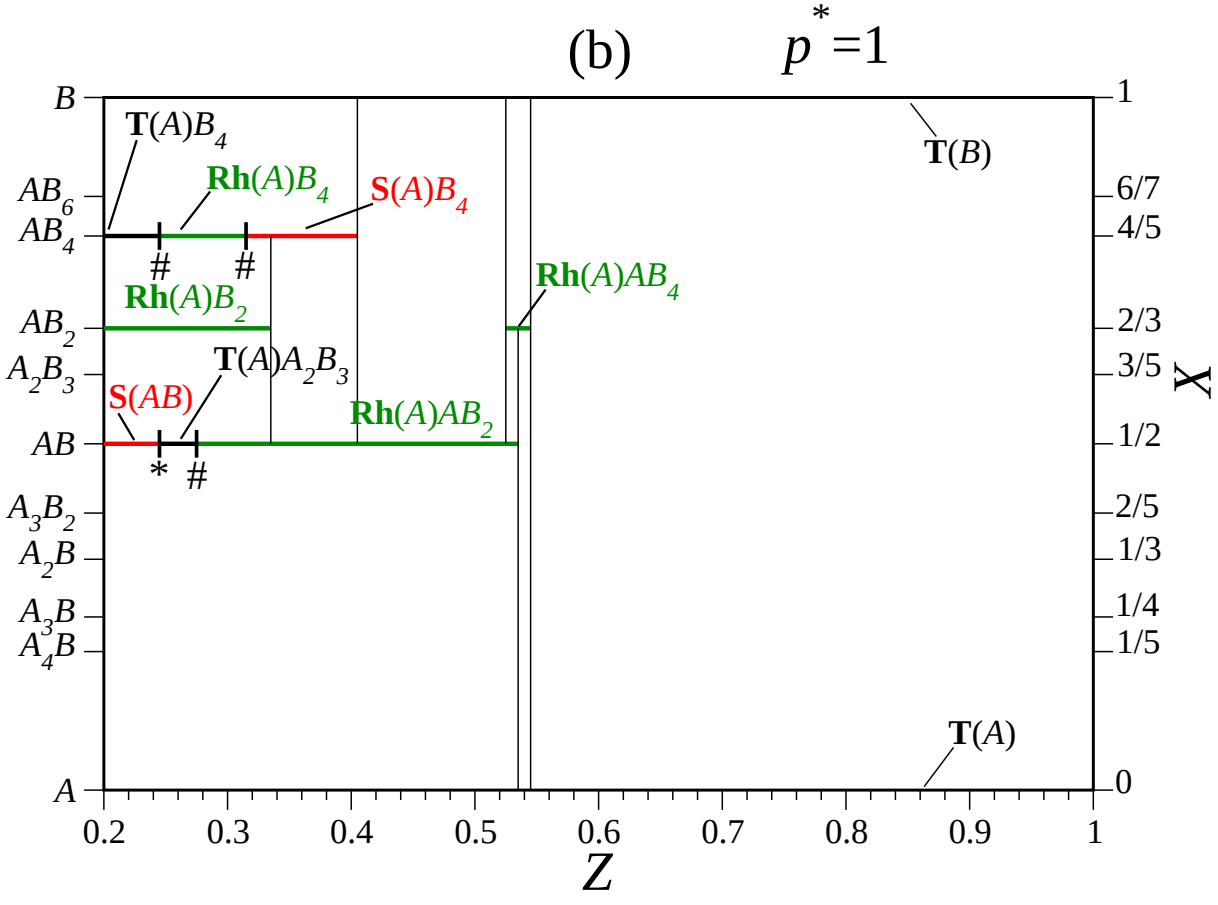
(b)
p^*=1
B
AB6
AB4
AB2
A2B3
AB
A3B2
A2B
A3B
A4B
A
1
6/7
4/5
2/3
3/5
1/2
2/5
1/3
1/4
1/5
0
T(B)
T(A)
T(A)B4
Rh(A)B4
S(A)B4
Rh(A)B2
Rh(A)AB4
T(A)A2B3
S(AB)
Rh(A)AB2
#
*
0.2
0.3
0.4
0.5
0.6
0.7
0.8
0.9
1
Z
X

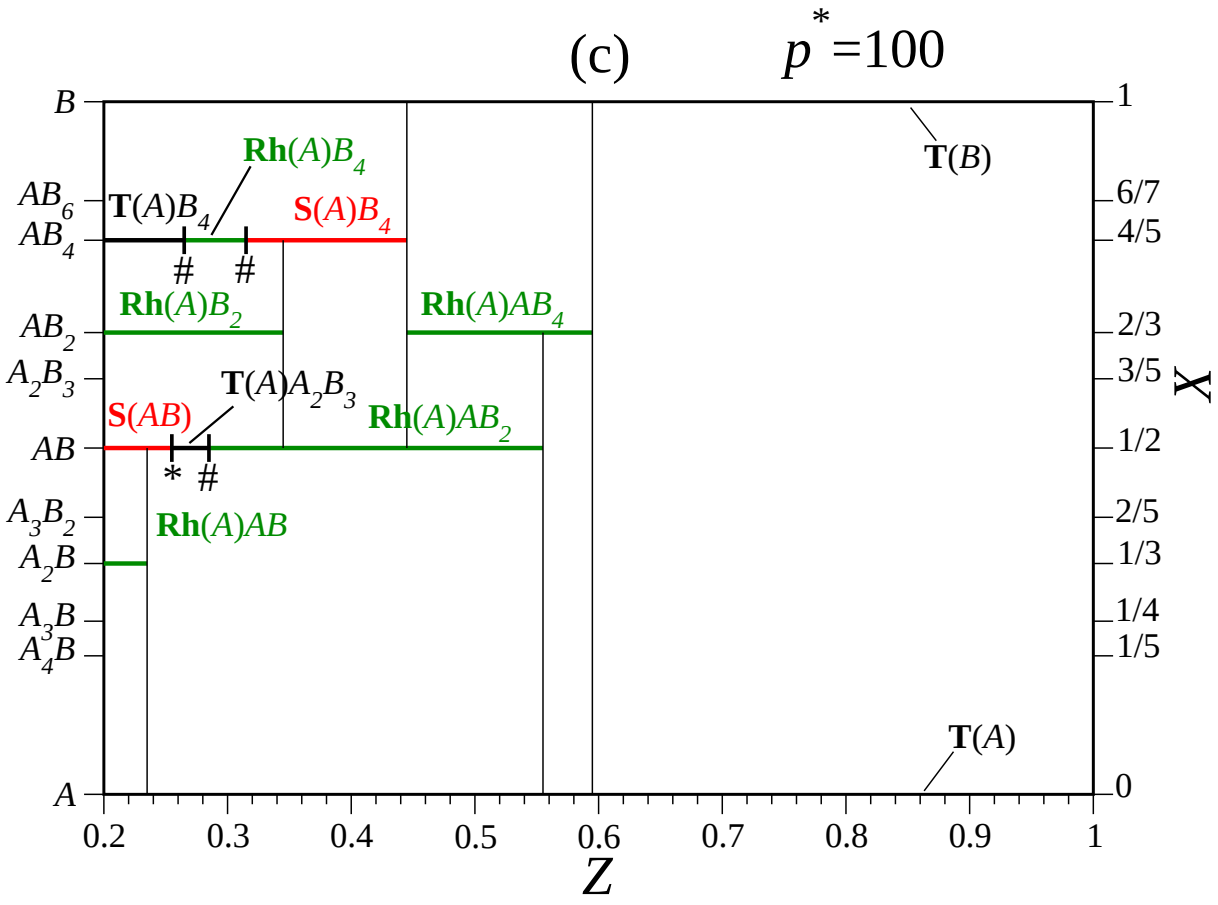

FIG. 2: The phase diagram in the (Z, X) plane of charge asymmetry and composition at $T = 0$ for a effective pressure (a) $p^* = 0.01$, (b) $p^* = 1$, (c) $p^* = 100$. The symbol # (∗) denote continuous (discontinuous) transitions.

separation reported in Fig. 2(c) for $p^* = 100$, where $\kappa^* \approx 0.4$ for large charge symmetry. Recently, we have shown for dipolar binary mixtures [9], whose pair potential is governed by $1/r^3$, that, at weak dipolar asymmetry (the analogous quantity to the charge ratio in our present study), the *stable mixtures* A_2B and AB_2 (who are globally triangular) set in. This phase behavior contrasts therefore strongly with that presently reported for Yukawa mixtures, see Fig. 2(c). Given the fact that at weak screening the Yukawa pair potential is well approximated by a $1/r$ dependence, which is even softer than $1/r^3$, it is legitimate to expect stable mixtures in the regime of weak screening and charge asymmetry. In order to check this idea we have performed additional calculations at $p^* = 10^{10}$ with $Z = 0.99$ leading to reduced screening strengths of the order of 10^{-2}. Those values for κ^* turn out to be still too large to recover the phase behavior found at $1/r^3$-pair interactions [9]. The

consideration of even much smaller screening strengths (say roughly of the order of 10^{-7}) are numerically not tractable within reasonable CPU time. Unfortunately, the implementation of a direct Lekner and/or Ewald sum for the $1/r$-pair interactions is delicate at *prescribed pressure*, since the lack of electroneutrality involves the presence of an artificial homogeneous neutralizing background which is thermodynamically only consistent at *prescribed density* [53]. Consequently, although we have a strong intuition about the stability of mixtures at weak charge asymmetry and screening, we can not prove it here on computational basis.

We now briefly address the more complicated phase behavior reported at strong charge asymmetry, see Fig. 2 with $Z \lesssim 0.5$. As a clear general trend, it is found that the number of stable phases increases with growing pressure. This feature is in agreement with the idea that mixing is favored upon softening the pair potential.

A common and remarkable feature in this regime of strong charge asymmetry (see Fig. 2) is the imposing stability of the composition $X = 1/2$. This feature was also reported for dipolar mixtures [9]. More specifically, the following cascade $\mathbf{S}(AB) \to \mathbf{T}(A)A_2B_3 \to \mathbf{Rh}(A)AB_2$ is found upon increasing Z, see Fig. 2 and Fig. 1 for the corresponding structures. Thereby, the transition $\mathbf{S}(AB) \to \mathbf{T}(A)A_2B_3$ is discontinuous whereas $\mathbf{T}(A)A_2B_3 \to \mathbf{Rh}(A)AB_2$ is continuous, see Fig. 2. Note that, for $p^* = 0.01$ shown in Fig. 2(a), the stability of the square phase $\mathbf{S}(AB)$ occurs for values of Z smaller than 0.2 that are not shown here.

B. Thermodynamical properties

1. Constant pressure

In this part, we investigate some thermodynamic properties such as the reduced density ρ^* or the reduced Gibbs free energy $g^* \equiv g/(V_0\kappa)$, as obtained prior the Maxwell construction. Although the pressure considered here is fixed at $p^* = 100$, very similar results are obtained for the two other pressures.

The reduced density ρ^* as a function of the charge ratio Z at different compositions X is sketched in Fig. 3. At given composition X, the density decreases monotonically with Z, see Fig. 3. This effect can be simply explained as follows: Upon increasing Z the repulsive $A-B$ and $B-B$ pair interactions increase accordingly, so that to keep the pressure fixed the system has to decrease its density. Moreover, at prescribed charge ratio, Fig. 3 indicates that

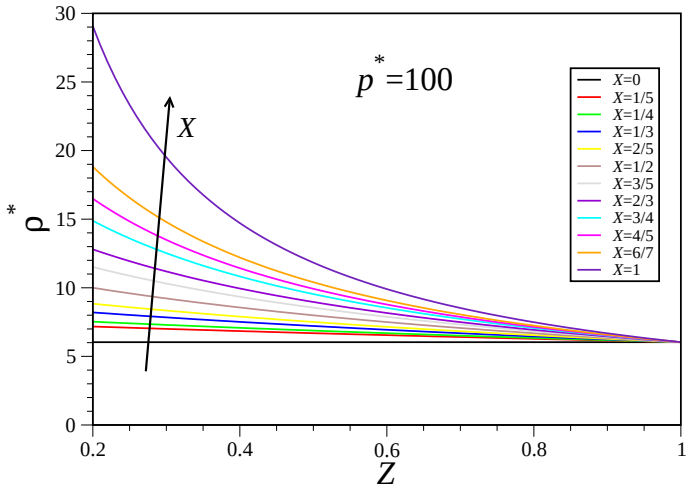

FIG. 3: Reduced density ρ^* (prior the Maxwell construction) as a function of the charge ratio Z for various compositions X at prescribed reduced pressure $p^* = 100$. The arrow indicates growing X.

the density increases with the composition. This feature can also be explained with simple physics: Upon enlarging the composition X, the proportion of *weakly* charged B-particles increases accordingly, so that to keep the pressure constant the system has to increase its density.

The reduced Gibbs free energy g^* as a function of the charge ratio Z at different compositions X is sketched in Fig. 4. Recalling that $g^* = u^* + p^*/\rho^*$ [with $u^* \equiv u/(V_0\kappa)$], the behavior of g^* exhibi cating the just

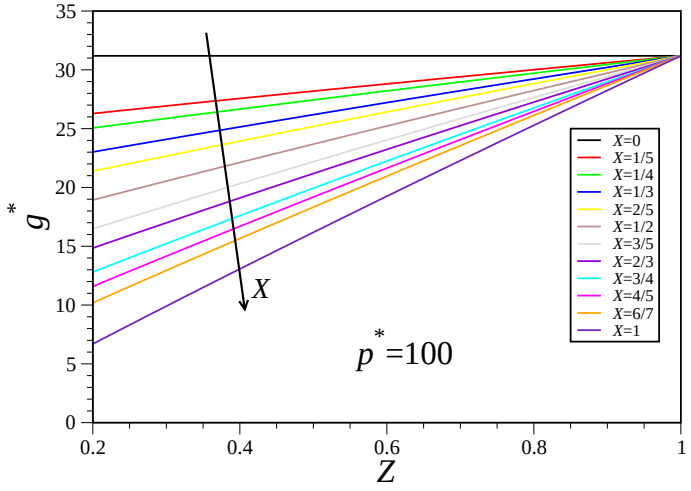

FIG. 4: Same as Fig. 3 but for g^*.

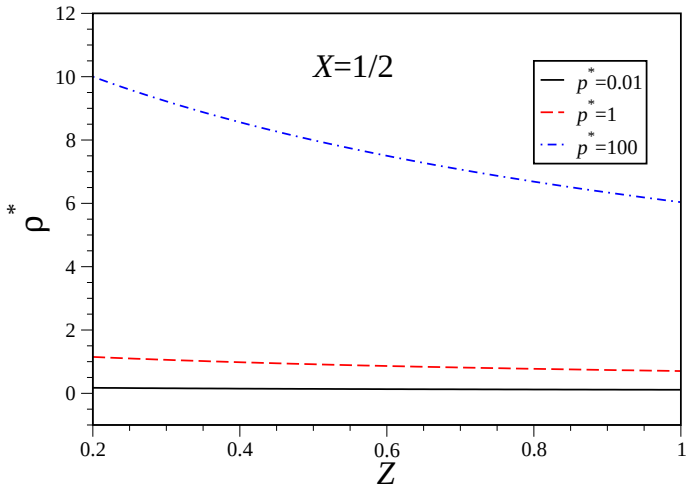

FIG. 5: Reduced density ρ^* (prior the Maxwell construction) as a function of the charge ratio Z for various reduced pressures p^* at prescribed composition $X = 1/2$.

explained behavior of ρ^* described in Fig. 3. Since the reduced internal energy u^* decreases with growing X and therefore with growing ρ^* at prescribed Z, it is clear that g^* decreases with growing X at given Z, as seen in Fig. 4. Besides, at given composition X, Fig. 4 shows that g^* increase with growing Z, as expected.

2. Constant composition

We now analyze ρ^* and g^* at $X = 1/2$ as a function of Z for different values of p^*. As far as the behavior of ρ^* is concerned, the new information provided by Fig. 5 is that ρ^* increases with growing pressure at given charge ratio, as it should be. The same qualitative feature is also observed for g^* in Fig. 6. A closer inspection of Fig. 5 and Fig. 6 suggests that ρ^* and g^* increase rather slowly with p^* (at given Z^*).

IV. CONCLUDING REMARKS

In conclusion we have determined the ground-state (i.e. zero-temperature) phase diagram for a two-component Yukawa monolayer at various pressure for arbitrary compositions and a broad range of charge asymmetries. Among a big number of candidate phases, a wealth of different composite lattices has been found to be stable. The larger the charge asymmetry, the more complex is the phase diagram. At low asymmetry the system shows demixing

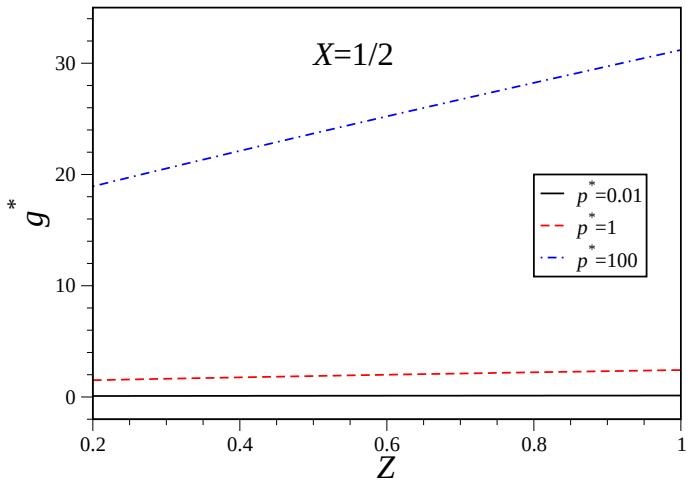

FIG. 6: Same as Fig. 5 but for g^*.

into pure A and B crystals similar to hard disks but different from the soft inverse cube interaction valid for dipoles. The results are in principle detectable in binary mixtures of charged colloids confined between two charged plates or levitated dusty plasma sheets.

It would be interesting to study the effect of finite temperature. We expect that the topology of the phase diagram does not change upon gently increasing the temperature though this could change close to melting. When cooling a two-component fluid down, glass formation in the binary systems at finite temperature may be a fascinating topic as well [54] to be studied in the future. In fact, it has been speculated that the underlying crystallization into the stable crystal lattices may control vitrification [55] and therefore are findings are relevant for the structure of glasses as well.

Acknowledgments

We thank T. Palberg and H. Tanaka for helpful discussions. This work was supported by the DFG via the SFB TR6 (project section D1).

APPENDIX A: LEKNER SUMS FOR YUKAWA INTERACTIONS IN TWO DIMENSIONAL SYSTEMS

We consider a primitive cell in the shape of a parallelogram, which contains a set of $n = n_A + n_B$ particles interacting via Yukawa potentials. The parallelogram repeated in

the xy plane gives a 2-dimensional lattice, and can be described by two lattice vectors $\mathbf{a} = (a_x, 0)$ and $\mathbf{b} = (b_x, b_y)$. In the parallelogram, the position of a charge valency Z_i is defined by $\mathbf{r}_i = (x_i, y_i)$.

The total interaction energy per cell is given by

$$\frac{U}{V_0} = \frac{1}{2}\sum_{i=1}^{n}\sum_{j\neq 1}^{n} Z_i Z_j \Phi(\mathbf{r}_{ij}) + \frac{1}{2}\sum_{i=1}^{n} Z_i^2 \Phi_0 \tag{A1}$$

with

$$\Phi(\mathbf{r}) = \sum_{\mathbf{R}} \frac{\exp(-\kappa|\mathbf{r}+\mathbf{R}|)}{|\mathbf{r}+\mathbf{R}|} \quad \text{and} \quad \Phi_0 = \sum_{\mathbf{R}\neq 0} \frac{\exp(-\kappa|\mathbf{R}|)}{|\mathbf{R}|}, \tag{A2}$$

where

$$|\mathbf{r}+\mathbf{R}| = \sqrt{(x+a_x l + b_x m)^2 + (y+b_y m)^2} \quad \text{and} \quad |\mathbf{R}| = \sqrt{(a_x l + b_x m)^2 + (b_y m)^2}.$$

Here $\mathbf{R} = l\mathbf{a} + m\mathbf{b}$ with l and m being integers. The slowly convergent sums over lattice sites (Eq. A2) can not be efficiently used in a numerical calculation, so that we will transform them into rapidly convergent forms using a Lekner Method [56, 57]. With the help of the following integral representation

$$\frac{\exp(-\kappa|\mathbf{r}+\mathbf{R}|)}{|\mathbf{r}+\mathbf{R}|} = \frac{1}{\sqrt{\pi}}\int_0^\infty \frac{dt}{\sqrt{t}} \exp\left(-\frac{\kappa^2}{4t} - |\mathbf{r}+\mathbf{R}|^2 t\right), \tag{A3}$$

we obtain

$$\Phi(\mathbf{r}) = \frac{1}{\sqrt{\pi}}\int_0^\infty \frac{dt}{\sqrt{t}} \left\{ \exp(-\frac{\kappa^2}{4t}) \sum_{m=-\infty}^{\infty}\sum_{l=-\infty}^{\infty} \exp\left[-(y+mb_y)^2 t\right] \exp\left[-\left(\frac{x}{a_x} + l + m\frac{b_x}{a_x}\right)^2 a_x^2 t\right] \right\}. \tag{A4}$$

Now, to get further, we apply a 1-dimensional Poisson summation

$$\sum_{l=-\infty}^{\infty} \exp\left[-(\alpha+\beta l)^2 t\right] = \frac{\sqrt{\pi}}{\beta\sqrt{t}} \sum_{k=-\infty}^{\infty} \exp\left(i2\pi k\frac{\alpha}{\beta}\right) \exp\left(-\frac{\pi^2 k^2}{\beta^2}\frac{1}{t}\right), \tag{A5}$$

which provides

$$\sum_{l=-\infty}^{+\infty} \exp\left[-(\frac{x}{a_x} + l + m\frac{b_x}{a_x})^2 a_x^2 t)\right] = \frac{1}{|a_x|}\sqrt{\frac{\pi}{t}} \left[1 + 2\sum_{k=1}^{+\infty} \cos\left[2\pi k\left(\frac{x}{a_x} + m\frac{b_x}{a_x}\right)\right] \exp\left(-\pi^2 k^2/a_x^2 t\right)\right]. \tag{A6}$$

Inserting Eq. (A6) into Eq. (A4) yields:

$$\begin{aligned}\Phi(\mathbf{r}) \;=\; & \frac{1}{|a_x|}\sum_{m=-\infty}^{\infty}\int_0^{\infty}\frac{dt}{t}\exp\left[-\frac{\kappa^2}{4t}-(y+mb_y)^2t\right] \\ & +\frac{2}{|a_x|}\sum_{k=1}^{+\infty}\sum_{m=-\infty}^{+\infty}\cos\left[2\pi k\left(\frac{x}{a_x}+m\frac{b_x}{a_x}\right)\right] \\ & \times\int_0^{\infty}\frac{dt}{t}\exp\left[-\left(\kappa^2+\frac{4\pi^2k^2}{a_x^2}\right)\frac{1}{4t}-(y+mb_y)^2t\right] \end{aligned} \tag{A7}$$

Now, taking into account the following relation

$$\int_0^{\infty}\frac{dt}{t}\exp\left(-\frac{B^2}{4t}-C^2t\right)=2K_0(BC) \tag{A8}$$

where K_0 is the zeroth order modified Bessel function of the second kind, The final expression for $\Phi(\mathbf{r})$ reads:

$$\begin{aligned}\Phi(\mathbf{r}) \;=\; & \frac{2}{|a_x|}\sum_{m=-\infty}^{+\infty}K_0\left(\kappa|y+mb_y|\right) \\ & +\frac{4}{|a_x|}\sum_{k=1}^{\infty}\sum_{m=-\infty}^{+\infty}\cos\left[2\pi\left(\frac{x}{a_x}+m\frac{bx}{a_x}\right)\right] \\ & \times K_0\left[|y+mb_y|\sqrt{\kappa^2+\frac{4\pi^2k^2}{a_x^2}}\right] \qquad \text{for } y\neq 0 \end{aligned} \tag{A9}$$

and the "self" contribution Φ_0

$$\begin{aligned}\Phi_0 \;=\; & \frac{4}{|a_x|}\sum_{m=1}^{\infty}K_0(\kappa mb_y) \\ & +\frac{8}{|a_x|}\sum_{k=1}^{\infty}\sum_{m=1}^{\infty}\cos\left(2\pi km\frac{bx}{a_x}\right)K_0\left[mb_y\sqrt{\kappa^2+\frac{4\pi^2k^2}{a_x^2}}\right] \\ & -\frac{2}{|a_x|}\ln\left[1-\exp(-\kappa a_x)\right] \end{aligned} \tag{A10}$$

In the limit of a rectangular based cell, i.e setting $b_x = 0$, one obtains the formulas for the cross and self-energies that are identical to those derived in [57] with $z = 0$.

---

[1] G. Tammann, Ann. d. Physik. **40**, 237 (1913).

[2] S. Pronk and D. Frenkel, Phys. Rev. Lett. **90**, 255501 (2003).

[3] H. Xu and M. Baus, J. Phys: Condens. Matter **4**, L663 (1992).

[4] M. D. Eldridge, P. A. Madden, and D. Frenkel, Nature **365**, 35 (1993).

[5] P. Bartlett, R. H. Ottewill, and P. N. Pusey, Phys. Rev. Lett. **68**, 3801 (1992).

[6] J. Hafner, *From Hamiltonians to Phase Diagrams* (Springer, Berlin, 1987).

[7] G. Gompper and M. Schick, *Soft Matter, Vol. 2: Complex Colloidal Suspensions* (WILEY-VCH Verlag GmbH and Co. KGaA, Weinheim, 2006).

[8] C. N. Likos and C. L. Henley, Philos. Mag. B **68**, 85 (1993).

[9] L. Assoud, R. Messina, and H. Löwen, Europhys. Letters **80**, 48001 (2007).

[10] J. Fornleitner, F. Lo Verso, G. Kahl and C. N. Likos. To be published.

[11] M. B. Hay, R. K. Workman, and S. Manne, Phys. Rev. E **67**, 012401 (2003).

[12] K. Zahn, J. M. MendezAlcaraz, and G. Maret, Phys. Rev. Lett. **79**, 175 (1997).

[13] Y. Rosenfeld, Phys. Rev. E **47**, 2676 (1993).

[14] A. A. Louis, E. Allahyarov, H. Löwen, and R. Roth, Phys. Rev. E **65**, 061407 (2002).

[15] E. Scholl-Paschinger and G. Kahl, J. Chem. Phys. **118**, 7414 (2003).

[16] P. Hopkins, A. J. Archer, and R. Evans, J. Chem. Phys. **124**, 054503 (2006).

[17] J. Kofinger, N. B. Wilding, and G. Kahl, J. Chem. Phys. **125**, 234503 (2006).

[18] M. A. Chavez-Rojo and M. Medina-Noyola, Physica A: Statistical Mechanics and its Applications **366**, 55 (2006).

[19] N. Kikuchi and J. Horbach, Europhys. Letters **77**, 26001 (2007).

[20] G. Salin and D. Gilles, J. Phys. A: Math. Gen. **17**, 4517 (2006).

[21] H. Löwen, J. Phys.: Condens. Matter **4**, 10105 (1992).

[22] R. Messina and H. Löwen, Phys. Rev. Lett. **91**, 146101 (2003).

[23] P. Hartmann, G. J. Kalman, and K. K. Z. Donko, Phys. Rev. E **72**, 026409 (2005).

[24] P. Hartmann, G. Z. Kalman, and Z. Donko, J. Phys. A: Math. Gen. **39**, 4485 (2006).

[25] K. Nelissen, B. Partoens, and F. . M. Peeters, Europhys. Letters **79**, 66001 (2007).

[26] B. Liu and J. Goree, Phys. Rev. E **75**, 016405 (2207).

[27] A. Libal, C. Reichhardt, and C. J. O. Reichhardt, Phys. Rev. E **75**, 011403 (2007).

[28] G. J. Kalman, P. Hartmann, Z. Donko, and M. Rosenberg, Phys. Rev. Lett. **92**, 065001 (2004).

[29] B. Liu and J. Goree, Phys. Rev. Lett. **94**, 185002 (2005).

[30] J. M. Mendez-Alcaraz, M. Chavez-Paez, B. D'aguanno, and R. Klein, Physica A **15**, 173 (1995).

[31] J. J. Gray and R. T. Bonnecaze, Langmuir **17**, 7935 (2001).

[32] A. Wysocki and H. Löwen, J. Phys.: Condens. Matter **16**, 7209 (2004).

[33] J. Dzubiella, G. P. Hoffmann, and H. Löwen, Phys. Rev. E **65**, 021402 (2002).

[34] C. Desgranges and J. Delhommelle, J. Chem. Phys. **126**, 054501 (2007).

[35] E. Allahyarov, H. Löwen, and S. Trigger, Phys. Rev. Lett. **57**, 5818 (1998).

[36] O. S. Vaulina and I. E. Dranzhevskii, Plasma. Phys. Reports **33**, 494 (2007).

[37] C. A. Murray and D. H. van Winkle, Phys. Rev. Lett. **58**, 1200 (1987).

[38] M. Brunner *et al.*, Europhys. Letters **58**, 926 (2002).

[39] A. B. Fontecha *et al.*, J. Phys.: Condens. Matter **17**, S2779 (2005).

[40] E. Chang and D. Hone, Europhys. Letters **5**, 635 (1988).

[41] E. Allahyarov, I. D'Amico, and H. Löwen, Europhys. Letters **5**, 635 (1988).

[42] C. R. Nugent, H. N. P. K. V. Edmond, and E. R. Weeks, Phys. Rev. Lett. **99**, 025702 (2007).

[43] N. Hoffmann, F. Ebert, C. N. Likos, and G. M. H. Löwen, Phys. Rev. Lett. **97**, 078301 (2006).

[44] M. H. Kong, B. Partoens, and F. . M. Peeters, New J. of Phys. **5**, 494 (2003).

[45] G. P. Hoffmann and H. Löwen, J. Phys: Condens. Matter **12**, 7359 (2000).

[46] V. Nosenko, S. Nunomura, and J. Goree, Phys. Rev. Lett. **88**, 215002 (2002).

[47] V. Nosenko *et al.*, Phys. Rev. E **68**, 056409 (2003).

[48] H. Totsuji, T. Kishimoto, C. Totsuji, and T. Sasabe, Phys. Rev. E **58**, 7831 (1998).

[49] V. N. Manoharan, T. Elsesser, and D. J. Pine, Science **301**, 483 (2003).

[50] J. Kecht *et al.*, Langmuir **20**, 5271 (2004).

[51] F. Yan and W. A. Goedel, Chem. Mater. **16**, 1622 (2004).

[52] A. E. Saunders and B. A. Korgel, ChemPhysChem **6**, 61 (2005).

[53] L. Bonsall and A. A. Maradudin, Phys. Rev. B **15**, 1959 (1977).

[54] T. Hamanaka and A. Onuki, Phys. Rev. E **74**, 011506 (2006).

[55] T. Kawasaki, T. Araki, and H. Tanaka, Phys. Rev. Lett. **99**, 215701 (2007).

[56] J. Lekner, Physica A **157**, 826 (1989).

[57] M. Mazars, Mol. Phys. **105**, 1927 (2007).